Buildability assessment of 3D printed concrete elements through computer vision

Shanmugaraj Senthilnathan[1*] and Benny Raphael[2]

[1,2]Civil Engineering Department, Indian Institute of Technology Madras, India

[1*]ce20d005@smail.iitm.ac.in, [2]benny@iitm.ac.in

Abstract –

Concrete 3D printing is a digital fabrication technology that has the potential to increase the level of automation in construction. However, getting consistent output quality is a challenge in concrete 3D printing because of the change in material properties with time and the influence of environmental parameters. A robust quality monitoring and control system is required to control the variations and obtain good-quality output. In this study, computer vision techniques are used to monitor the 3D printing process. Image features such as temporal variations in layer thickness and textural changes are used to assess the buildability properties. Two metrics have been developed for quantifying these features: entropy standard deviation and maximum layer thickness deformation. A significant correlation is found between the two metrics, and this relationship can be used to re-confirm the buildability assessment. For a given concrete mix, limiting values can be computed for the metrics to effectively classify an element into a stable type or one that is likely to collapse. This data can also be used as feedback to the printing system to make corrective actions to increase the quality of the print output. Thus, a real-time, non-intrusive buildability assessment system for concrete 3DP elements is demonstrated in this study.

Keywords –

Concrete 3D printing; Computer Vision; Buildability,; Quality monitoring

1 Introduction and background

Concrete 3D printing (3DP) is a freeform technology that aims to realize the benefits of digital fabrication. It has been found to reduce construction time, material, and labor usage while improving sustainability. However, due to the dependency of material properties on multiple input parameters, 3D printed elements are found to have variations in the output quality. 3D printing challenges include proper extrusion and limiting dimensional changes with time [1]. One of the critical parameters of 3DP is buildability, which determines the number of layers that can be printed without significant dimensional changes in individual layers due to the weight of the top layers. The common buildability failures in 3D printing are plastic and buckling collapse [2]. It depends mainly on the workability of the concrete, and many studies have used fresh-state property tests to find a printable region.

There are very few real-time techniques that help in monitoring the variations during the printing process. Studies on quality monitoring and control techniques are increasing in the additive manufacturing industry [3]. However, studies on quality monitoring in concrete 3DP are relatively less. Monitoring using 2D camera images and computer vision techniques is gaining prominence in industry applications. In this study, a computer vision methodology for quality monitoring is developed that helps assess the buildability properties of 3D printed elements. Significant dimensional changes affect the print quality and long-term structural properties [4,5]; hence these are monitored in this methodology. In addition, new image features have been identified that can effectively assess the buildability properties of 3DP elements.

2 Methodology

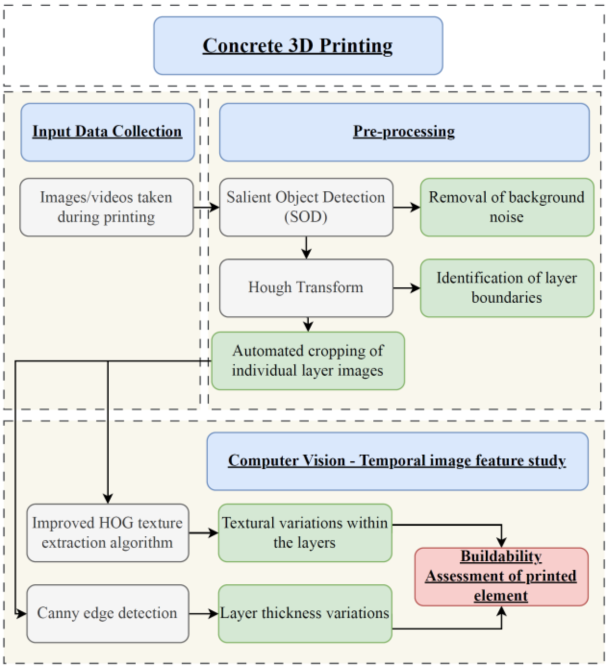

Figure 1. Methodology of buildability assessment using image features extracted through computer vision techniques

Figure 1 shows the overall methodology for buildability assessment of 3D printed elements using Computer Vision (CV). It consists of the following three parts:

- Input data collection
- Image pre-processing
- Study of temporal image features

In the input data collection phase, 2D images of the 3D-printed elements are collected using a camera during printing. The input data is preprocessed in the second stage to remove all the background data, reducing the computational complexity and increasing accuracy. The final phase involves the usage of computer vision techniques to extract image features and understand the temporal variations of the image features. The temporal variations are used to assess the buildability and the dimensional changes in the printed elements.

3 Materials and Methods

3.1 Experimental procedure

To demonstrate the methodology for buildability assessment using computer vision, a series of elements were printed in a laboratory setting. The experimental details are described in this section.

This study uses a new LC2-OPC mix, which uses Limestone Calcined Clay (LC2) and Ordinary Portland Cement (OPC) cement as binders with manufactured sand as aggregate. Super-plasticizers (SP) and viscosity modifying agents (VMA) are used to control the rheological properties of the printed elements. In general, buildability properties depend on the rheological properties, especially the workability of the printing concrete. The initial workability of concrete varies with super-plasticizer dosage. However, the workability during the printing process is dynamic, with variations occurring due to hydration or evaporation with time. Hence, elements are printed under different initial workability conditions and at different times of printing (time from the point of mixing water to the dry concrete mix) to understand the impact of the changes in rheological properties on the buildability of 3DP elements.

Table 1. 3DP elements printed with different Super-Plasticizer (SP) and Time Of Printing (TOP) as per experimental procedures

Category No.	SP (%)	TOP (min)	Status of Print
1		10-15	Collapsed
2	0.50	25-30	Collapsed
3		40-45	Good quality print with slight expansion/distortion in the middle
4		10-15	Good print with minor voids in the top layers
5	0.40	25-30	Fair print with many voids in the top layers
6		40-45	Non-extrudable
7		10-15	Good print with a fair amount of voids in the top layers
8	0.30	25-30	Non-extrudable
9		40-45	Non-extrudable

Table 1 shows the elements printed with different super-plasticizer values of 0.50%, 0.40%, and 0.30% to account for initial workability changes. For every super-plasticizer (SP) dosage, the Time of Printing (TOP) is varied in three ranges, 10-15, 25-30, and 40-45 mins. The different TOP values account for dynamic workability changes during the printing process. Nine different categories of printing were done as part of the experimental procedure. For every category, three prints were done to capture the variation in the data. For

Category 1 and 2, the super-plasticizer dosage was very high, resulting in collapse before reaching the target height of 500 mm. The super-plasticizer value was very low for categories 6, 8, and 9, making the concrete non-extrudable and non-printable. Since this is a buildability study, the non-extrudable categories are not considered.

A Canon 1300D 18MP camera was kept directly at the printing palette at a horizontal distance of 1000 mm from the printed element to capture the 2D video/images of the 3DP element. An illumination lamp was kept above the camera, which provides a constant illumination of 6500 (+/-100) Lux on the surface of the printed elements. The same camera and lighting setup were followed for all the print elements.

A stable element that retained shape and could be printed to a target height of 500 mm without collapse is designated as a good buildable element. If the element collapsed before the target height, it is classified as a collapsed or bad buildable element.

3.2 Image Data Collection and Pre-processing

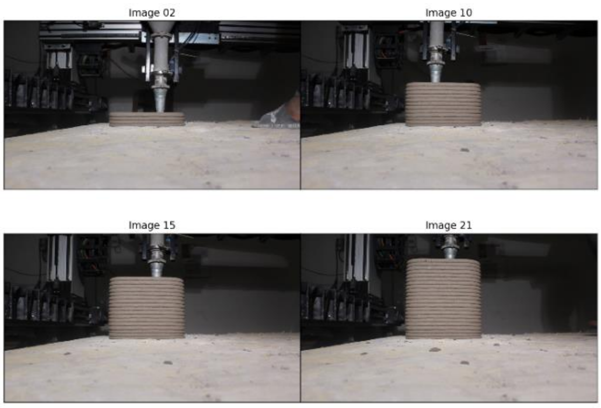

Figure 2. Input image of a stable 3D-printed Element - A

Figure 2 shows the input images of the 3D-printed element that reached the target height of 500 mm (Element A). Individual snapshots were taken from the video after the completion of every layer (layer time instances). The layers are designated as L01, L02, and so on, numbered from bottom to top. The two bottom layers, L01 and L02, were intentionally compressed against the printing palette to act as the base for printing. Hence, the analysis is done from layers L03 to L10. Image 01 refers to the image instance captured after the completion of layer L03. Image 02 refers to the image instance captured after the completion of layer L04 and so on. The Image numbers – Image 01, Image 02, and so on refer to the image instances taken after the completion of every layer, and they indirectly represent the time of printing containing information about temporal changes in the overall printed element.

The input images are pre-processed to remove all the background data. It is first processed through Salient Object Detection (SOD) to segment only the objects in focus. All the objects outside the focus were removed and were converted into black pixels. Individual layers are cropped out, and their temporal changes are studied to extract useful image features.

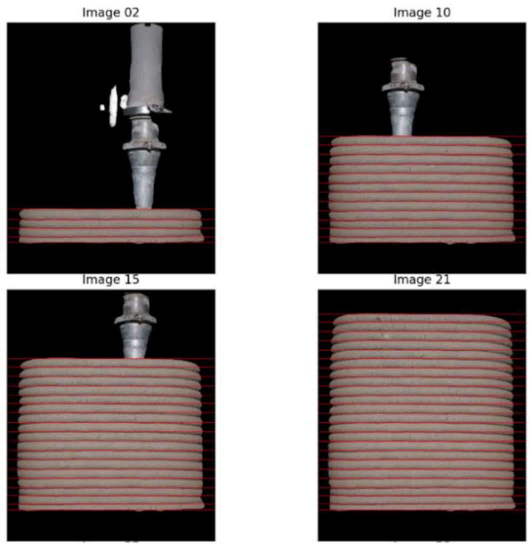

Figure 3. Hough Transform output after pre-processing of images of Element A

Each layer is characterized by the top and bottom layer boundaries, which are effectively horizontal for linear elements. Hence, the Hough Transform technique is used to identify the layer boundary [6]. Then, additional rows of pixels are added to the top and bottom boundaries to account for undulations in layer boundaries to crop the individual layers. Figure 3 shows the pre-processing output where all the background data is removed, and only the printed element is cropped out. It also shows the Hough Transform output, where all the layer boundaries are identified as horizontal red lines.

The image of each layer is obtained by cropping the initial image of the layer instance using the boundaries identified through Hough Transform. The temporal changes in each layer after the printing of subsequent top layers are captured within the crop window.

Figure 4. Temporal images of layer L03 of a good, stable printed Element A

Figure 5. Temporal images of layer L03 of a collapsed Element B

Figure 4 and Figure 5 show the temporal changes of layer L03 within a crop window for Elements A and B, respectively. The individual layer images are processed through two different computer vision techniques - texture analysis and layer thickness extraction; these are discussed in later sections.

It is found that the dimensional stability and the buildability of the printed element can be evaluated by assessing the bottom ten layers of every 3D printed element. Hence, only the bottom ten layers are used in the analysis.

3.3 Texture extraction – Modified Histogram of Oriented Gradients (HOG)

The texture is the tangible feel on the surface of the material. In the case of an image, it is computed as the variations in the brightness intensity of the pixels. This study uses a modified version of the Histogram of Oriented Gradients (HOG) concept. The modified HOG computes the gradient changes in three directions. The details of the concept and methods of the modified HOG algorithm are discussed in [7].

3.4 Entropy value calculation

Entropy is a measure of uniformity in a distribution. It was first introduced by Shannon and is given by the following formula,

$$\text{Entropy} = -\sum P_i * \log_2 P_i \tag{1}$$

Where Pi is the probability of the i-th value in the distribution. Entropy can be used for quantifying the textural changes within an individual layer image [7,8]. The higher the entropy value, the higher the textural value, and vice versa.

3.5 Canny edge detection

Canny edge detection is an edge detection method that looks for sudden changes in the pixel brightness intensities.

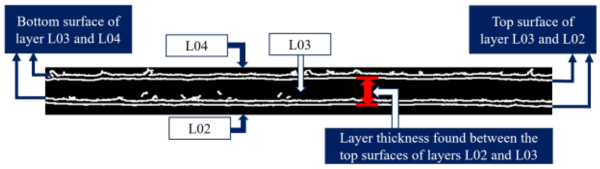

Figure 6. Canny edge detection output of L03 of Element A

Figure 6 shows the Canny edge detection output of layer L03 of Element A at a particular instance. It shows that the boundary lines between two layers are captured. The layer thickness is the vertical distance between the top and bottom boundaries of the layer identified from the Canny edge detection output. Two edge lines are determined for every boundary because the pixel intensity changes on both sides of a layer boundary. The layer thickness is computed as the vertical distance between the top surface boundary of the target layer to the bottom layer. It is done to avoid the impact of voids on the bottom surface boundary of individual layers.

4 Results and Discussions

4.1 Temporal textural variation

Figure 7 shows the temporal changes in the texture of the layer L03 of Element A. It is found that layer L03 deforms minimally from Image 02 to Image 20. Beyond that, no significant dimensional changes are visible within the crop window. The black pixels in Figure 7 represent the gradient (change in pixel intensities) observed within the layer L03 crop window, as obtained from the modified HOG algorithm. The number of black pixels within the L03 crop window is found to be changing from Image 02 to Image 20. Beyond that, it is consistent. This trend matches the pattern found in the actual dimensional changes within the crop window.

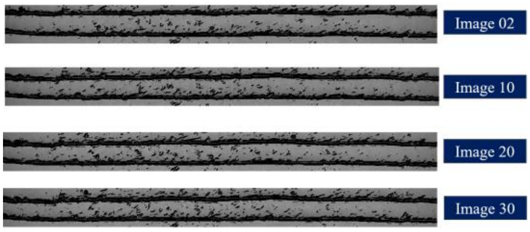

Figure 7. Temporal changes in the textural output of layer L03 of Element A

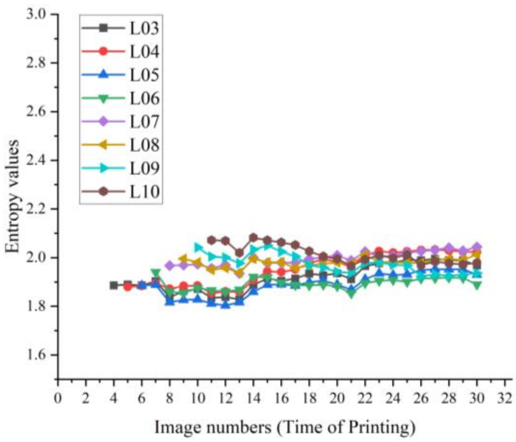

Figure 8. Temporal changes in the texture of layers L03 to L10 of Element A

The variations in the pixel intensities (gradient/black pixels) are captured as a single entropy value for each image instance. Its temporal changes are given in Figure 8. It is seen that the entropy values have minor variations until Image 20. Beyond that point, the values are constant, indicating that layer L03 has become stable by achieving the initial stiffness/yield strength.

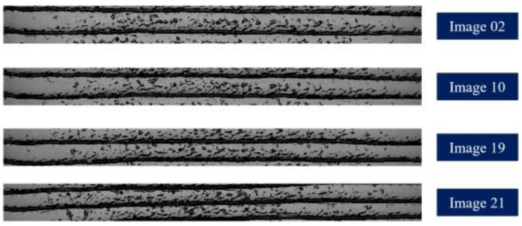

Figure 9. Temporal changes in the textural output of layer L03 of Element B

Figure 9 shows the modified HOG output of layer L03 of Element B. In contrast to Figure 7, the layer L03 of element B is continuously compressed with time. In Image 21, even the top layer has come into the crop window. This element eventually collapsed due to large deformations. The same is visible in the textural changes in terms of the number of black pixels varying with time (image instances).

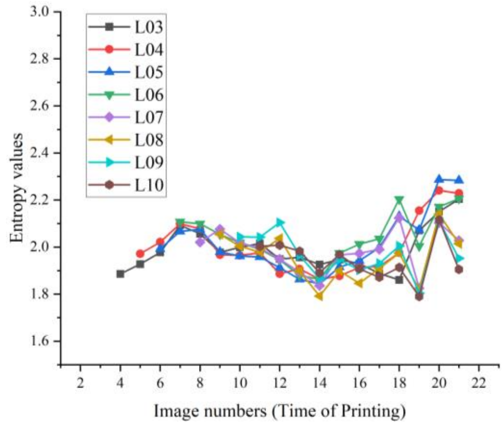

Figure 10. Temporal changes in the texture output of layers L03 to L10 of Element B

The temporal change in the texture of Element B is captured in terms of entropy value variations, as shown in Figure 10. Unlike Figure 8, the entropy values keep changing drastically and do not seem to consolidate.

Entropy Standard Deviation (ESD), or the standard deviation of the entropy values over time, is introduced in this study as a single measure of the temporal changes in entropy value for every individual layer. The standard deviation of entropy values (ESD) of layer L04 of element B is 0.1148, whereas the ESD value of layer L04 of element A is 0.0172. Similarly, ESD values for layers L03 to L10 of all the print elements. It is found that the ESD values are low for a stable print element and high for a collapsed print element. It proves that the ESD is a good measure of the dimensional stability or the buildability collapse assessment of the 3DP elements.

4.2 Temporal layer thickness variation

In continuation to section 3.5, the layer thickness is measured as the vertical distance between the two boundary edge lines identified from the Canny edge detection output. The layer thickness is found at thirty different sections along the line of printing. It is done to understand the layer thickness changes at different local sections rather than the overall average layer thickness. Figure 11 shows the layer thickness found in thirty different sections of layer L03 of Element A, identifying the layer boundaries and the vertical distance between them in terms of pixel points. Also, the changes in layer thickness over time are obtained by following the same steps on individual layer images taken at different time instances.

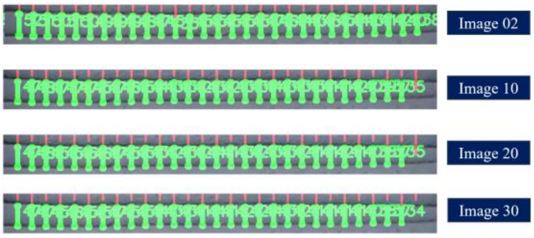

Figure 11. Layer thickness extracted at 30 different sections of layer L03 of Element A

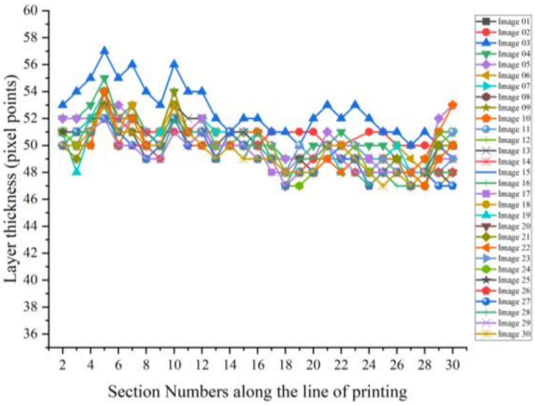

Figure 12. Layer thickness extracted at different sections of layer L03 of Element A

The changes in layer thickness are captured and shown in terms of a graph in Figure 12. The x-axis shows the different section points along the line of printing (where layer thickness is measured), and the y-axis shows the layer thickness in terms of pixel point units of layer L03 of element A measured at different time instances (Image numbers). The figure shows that the layer thickness initially reduces with time (increase in Image numbers). However, the layers gain initial stiffness/ yield strength with time, and the thickness reduction stabilizes.

Figure 13. Layer thickness extracted at different sections of layer L03 of Element B

The layer thickness found for layer L03 of Element B is given in Figure 13. Since the printed elements have high workability, the layer thickness continuously reduces with time, ultimately leading to the element's collapse.

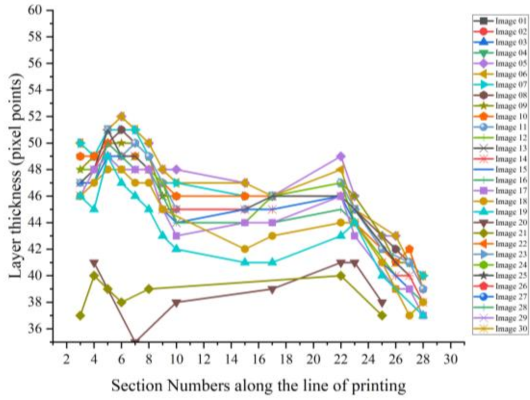

Figure 14. Layer thickness extracted at different sections of layer L03 of Element B

The temporal layer thickness changes of layer L03 of element B are given in Figure 14. Unlike Figure 12, the layer thickness value reduces continuously with time. Beyond Image 19, there is a sudden decrease in the layer thickness, ultimately leading to the element's collapse beyond the time instance - Image 22.

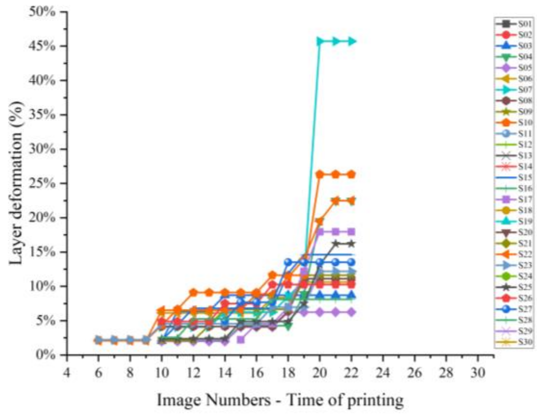

Figure 15. Layer Deformation (%) (LTD) of layer L03 of Element B

To have a single metric for layer thickness reduction, the concept of maximum Layer Thickness Deformation (LTD) (%) is introduced, where LTD is measured using the following formula:

LTD (%) = (Layer thickness at initial instance – layer thickness at instance X) / Layer thickness at initial instance X 100. (2)

The LTD is calculated at every section and every time instance X. The maximum deformation value across the different sections and the time instances is considered the Maximum LTD (MLTD) value. The LTD values found at different sections and different time instances of layer L03 of Element B are given in Figure 15. It shows the LTD values and their temporal changes (image numbers) across different sections along the printing line. It is found that the LTD values increase even beyond Image 16 and reached the maximum value at section 07 (MLTD) before the element's collapse. The MLTD value for layer L03 of Element B is 45.47%, but in the case of layer L03 of Element A, it is only 12.50%. The MLTD values are found for layers L03 to L10 of all the experimental print elements. It is found that the MLTD values of layers from a stable printed element are low. And for the collapsed element, the MLTD values are drastically high. Hence, MLTD also serves as a good image feature to assess the buildability collapse or dimensional stability of 3D printed elements.

4.3 Limiting value for entropy standard deviation (ESD)

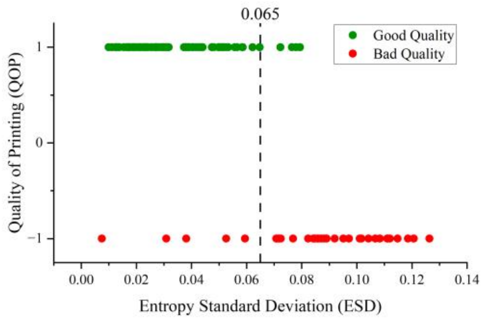

Figure 16. ESD vs. QOP plot showing the individual layer data points of good and bad quality printed element layers.

To find a limiting value that classifies a print element as a stable or collapsed element, each layer (L03 to L10) of all the experimental prints is considered as individual data points and analyzed. The layers L03 to L10 of a stable printed element are tagged as good-quality data points (Quality of Printing). In the case of collapsed print, all the individual layer data points (L03 to L10) are designated as bad-quality data points (Quality of Printing). Figure 16 shows the plot of the Entropy Standard Deviation (ESD) vs the Quality of Printing (QOP) designated based on the dimensional stability of every individual layer data point. The limiting value (discriminant) is found to be **0.065** (black dotted line) for ESD, which differentiates a stable and collapsed print element. The overall misclassification is 8.432% for the 130 individual layer data points assessed in this study.

4.4 Limiting value for maximum layer thickness deformation (MLTD)

Figure 17 shows the MLTD vs. QOP plot showing the maximum layer thickness deformation (MLTD) (%) of the individual layers (L03 to L10) of stable and collapsed printed elements. Similar to finding the limiting value for ESD, the layers of collapsed elements are designated as bad-quality data points, and the layers of stable elements are designated as good-quality data points. The limiting value is found to be **12.50%** for MLTD, with a misclassification of only 4.769%.

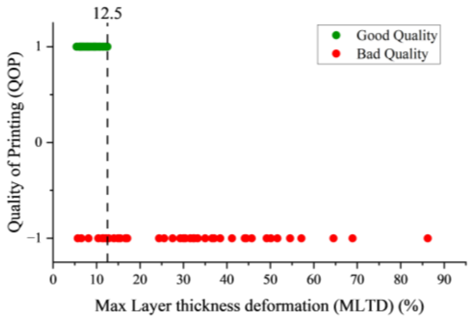

Figure 17. MLTD vs. QOP plot showing the good and bad quality individual layer data points

4.5 Relation between max layer thickness deformation (MLTD)(%) and entropy standard deviation (ESD)

Figure 18 shows the relation between the measured image feature metrics - MLTD (%) and ESD for all individual layer data points. All the individual layer data points from a stable printed element are given in green, and the collapsed printed element is given in red. A distinct region separation is noted from the plot. When the individual limiting values identified for each image feature are plotted, a discriminating boundary separating stable print data points and collapsed layer data points is found. It is to be noted that during the printing process, if any of the layers L03 to L10 falls in the collapse region or the rate of change of image feature values moves towards it, then there is a high chance of the 3D printed element collapsing. Hence, the correlation identified for ESD and MLTD can be used to supplement or re-confirm the buildability assessment from the individual image feature analysis. The developed limiting values of image features are valid for the current mix design and experimental procedures used in this study. They are not expected to vary drastically for other mixes as the dimensional change might be in the same pattern for collapse in other mixes.

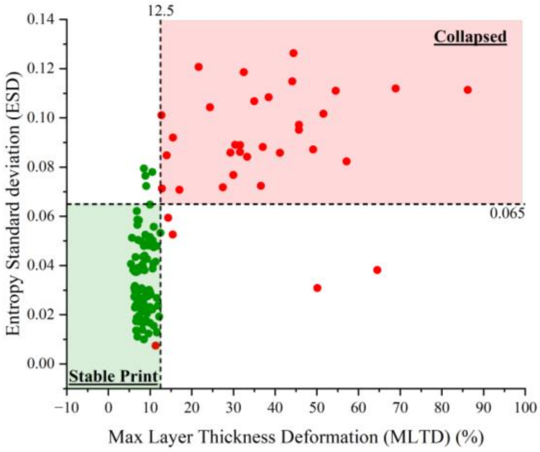

Figure 18. Plot showing the correlation between MLTD (%) and ESD

5 Conclusion

This paper presents a methodology for assessing the buildability of 3D printed concrete elements using computer vision techniques. Two new metrics have been developed in this research: Entropy Standard Deviation (ESD) and Maximum Layer Thickness Deformation (MLTD). These metrics are computed using image processing techniques and can be used for buildability assessment. The conclusions of the study are as follows:

- There exists a correlation between the two metrics. This relationship can be used to re-confirm the buildability assessment independently through two methods.
- For a given concrete mix, limiting values can be determined for the two metrics for discriminating between a stable print and one that could result in a collapse.
- Buildability or dimensional stability in terms of a stable/collapse print can be evaluated by monitoring and assessing the bottom ten printed layers of a single batch of concrete mix.

This is the first study to identify metrics that clearly predict properties of 3D printed concrete elements. This study paves the way for further research in computer vision on the use of image features to assess critical parameters like buildability. The image features can be used in a feedback loop to control the printing system. Based on the temporal variations in the image features, extrusion speed, and printing speed can be modified to give the bottom layers significant time to increase initial stiffness and yield strength to carry the weight of the top layers. It ensures sufficient buildability and avoids material wastage, increasing the sustainability of 3D printing technology. Thus, the study will help develop an autonomous, non-intrusive tool for the buildability assessment of concrete 3D-printed elements.

References

[1] A. Kazemian, X. Yuan, O. Davtalab, B. Khoshnevis, Automation in Construction Computer vision for real-time extrusion quality monitoring and control in robotic construction, Autom Constr 101 (2019) 92–98. https://doi.org/10.1016/j.autcon.2019.01.022.

[2] A.S.J. Suiker, R.J.M. Wolfs, S.M. Lucas, T.A.M. Salet, Elastic buckling and plastic collapse during 3D concrete printing, Cem Concr Res 135 (2020). https://doi.org/10.1016/j.cemconres.2020.106016.

[3] A. Oleff, B. Küster, M. Stonis, L. Overmeyer, Process monitoring for material extrusion additive manufacturing: a state-of-the-art review, Progress in Additive Manufacturing (2021) 23–27. https://doi.org/10.1007/s40964-021-00192-4.

[4] S. Lim, R.A. Buswell, P.J. Valentine, D. Piker, S.A. Austin, X. De Kestelier, Modelling curved-layered printing paths for fabricating large-scale construction components, Addit Manuf 12 (2016) 216–230. https://doi.org/10.1016/j.addma.2016.06.004.

[5] B. Raphael, S. Senthilnathan, A. Patel, S. Bhat, A review of concrete 3D printed structural members, Front Built Environ 8 (2023). https://doi.org/10.3389/fbuil.2022.1034020.

[6] L. Chandrasekar, G. Durga, International Conference on Communications and Signal Processing (ICCSP), in: 2014 International Conference on Communication and Signal Processing,IEEE, https://ieeexplore.ieee.org/document/6949962 (accessed March 8, 2024).

[7] S. Senthilnathan, B. Raphael, Quality monitoring of Concrete 3D Printed elements using computer vision-based texture extraction technique, in: 2023 Proceedings of the 40th ISARC, Chennai, India, 2023:pp.474–481. https://doi.org/10.22260/ISARC2023/0064.

[8] S. Senthilnathan, B. Raphael, Using Computer Vision for Monitoring the Quality of 3D-Printed Concrete Structures, Sustainability (Switzerland) 14 (2022). https://doi.org/10.3390/su142315682.